FOUNDATIONS AND APPLICATIONS OF THE EMPIRICAL SIMILITUDE METHOD (ESM)

Alan J. Dutson
Graduate Research Assistant

Kristin L. Wood
Cullen Trust Endowed Professor in Engineering

Department of Mechanical Engineering
The University of Texas at Austin
M/C C2200, ETC 4.146B
Austin, TX 78712-1063

SEPTEMBER 2002

ABSTRACT

Engineering design and manufacturing research have matured and evolved greatly over the last two decades. On the one hand, methods in engineering design are significantly impacting industry practice. They have also dramatically changed our classroom instruction and teaching pedagogies in engineering. On the other hand, new manufacturing processes have been commercialized and infused into production lines. These same processes are being used to prototype, quickly, our ideas in the engineering classroom.

Functional testing represents an important bridge between design and manufacturing processes. During product development, functional testing of models and prototypes offers significant advantages over direct product testing. However, two primary issues have historically prevented effective functional testing with prototypes: prediction accuracy and confidence in scale testing results.

The traditional similarity method, which is based on dimensional analysis, is commonly applied to perform scale testing. However, this method may not provide accurate scale testing results, especially when distortions exist, such as differences in available model and product material. This presentation focuses on an innovative empirical similarity method (ESM) to overcome such limitations. ESM is based on the premise of using specimen pairs to improve prediction accuracy. The theoretical foundations of this approach are presented, in addition to its relationship with traditional similitude and the bounds on its utility.

Based on ESM's theoretical development, two applications are presented. These applications include structural design of a basic cantilever member and design of a heat sink device. Empirical results are shown for the applications, including full-scale product testing.

1 Background

Product design and development processes recursively synthesize products that satisfy customer needs and functional requirements within limited temporal and financial resources (Pahl and Beitz, 1985; Ullman, 1992; Otto and Wood 2000). Companies continuously collect and analyze functional, aesthetic, ergonomic, and manufacturing information to produce quality products. The effort required to obtain such information is one of the key factors that determines the performance of the design process (Holmes, 1991; Ulrich and Eppinger 1995; Otto and Wood 2000).

Various types of virtual and physical models are utilized to provide proper functional information for a product. Virtual models are preferred to physical models in many cases because of their high flexibility, short development time, and relatively low cost. Despite significant advances in virtual modeling, however, the natural phenomena that can be accurately and confidently represented purely by virtual models are still very limited. Thus, companies typically utilize both virtual and physical models to verify and refine product designs.

During the last two decades various rapid prototyping techniques have been developed which produce geometrically complex physical models with significantly reduced fabrication effort. Considering the significant time and cost spent on product testing, it is natural to expect various industrial applications of rapid prototypes for functional testing. However, companies appear to utilize rapid prototypes mostly in the early design stages. Very few case studies are reported on functional testing with rapid prototypes (Dornfield, 1995; O'Reilly, 1993), with material limitations being a key factor (Wall et al., 1991). Similarity methods represent an opportunity to overcome these limitations and advance the state-of-the-art.

There exist primarily two types of similarity methods that correlate scaled prototypes and full-scale products: (1) the Buckingham Π theorem approach that correlates scaled model and product behaviors by considering dimensions of dominant system parameters (Bridgeman, 1931; Langhaar, 1951; Sedov, 1959; Szucs, 1980; Baker et al., 1991); and (2) an analytical approach that mathematically correlates the solutions of two known equations by comparing and manipulating the equations (Sedov, 1959; Kline, 1966; Bluman, 1986). The analytical approach can provide accurate scale testing results in general (Kline, 1965) but has limited application since it requires *a priori* knowledge of the governing equations for the system. The Buckingham Π approach (also know as dimensional analysis or the traditional similarity method, TSM) has a much wider range of application and is the approach considered in this paper.

Theory of TSM

The TSM states that two physically similar systems (a product *p* and a model *m*) whose behavior of interest *x* is influenced by the same governing parameters d_i, as in

$$x_p = f(d_1, d_2, ..., d_n) \qquad x_m = f(d_1, d_2, ..., d_n) \tag{1}$$

can be recast into an equivalent dimensionless form as follows:

$$\pi_{x,p} = g(\pi_{1,p}, \pi_{2,p}, ..., \pi_{N,p}) \qquad \pi_{x,m} = g(\pi_{1,m}, \pi_{2,m}, ..., \pi_{N,m}) \tag{2}$$

where $N < n$. Now,

$$\pi_{x,p} = \pi_{x,m} \; if \; \pi_{i,p} = \pi_{i,m} \; \forall \; i \tag{3}$$

Scale factors relating the governing parameters of the product to the corresponding parameters of the model can be determined from the similarity constraints in Eqn. 3. If all of the similarity constraints can be satisfied, the performance of the product can be predicted by testing the model and applying the appropriate scale factor.

Distortions in TSM (Model Distortions)

When the similarity constraints of two systems are not satisfied, the scaling between the two systems is said to be *distorted*; if the similarity constraints are satisfied, the systems are said to be *well-scaled*. We will refer to the distortion in scale factors between a product and a model as *model distortion*.

The theory of the TSM is valid only for those systems whose dimensionless parameters (π_i) are *exactly equal over the entire range of application*. This strict requirement of the TSM demands that all of the governing parameters be constant over the entire range of application (or, if there is variation in one of the governing parameters, that the variation be exactly equivalent in the corresponding parameter of the other system). Such strict requirements are often difficult to satisfy in practice. Cases in which the TSM requirements are not satisfied are summarized in Fig. 1. Any time a system includes one of the distortions listed in Fig. 1, the TSM no longer gives accurate predictions of product performance. Of course, the magnitude of the distortion will determine the magnitude of the error in the TSM prediction.

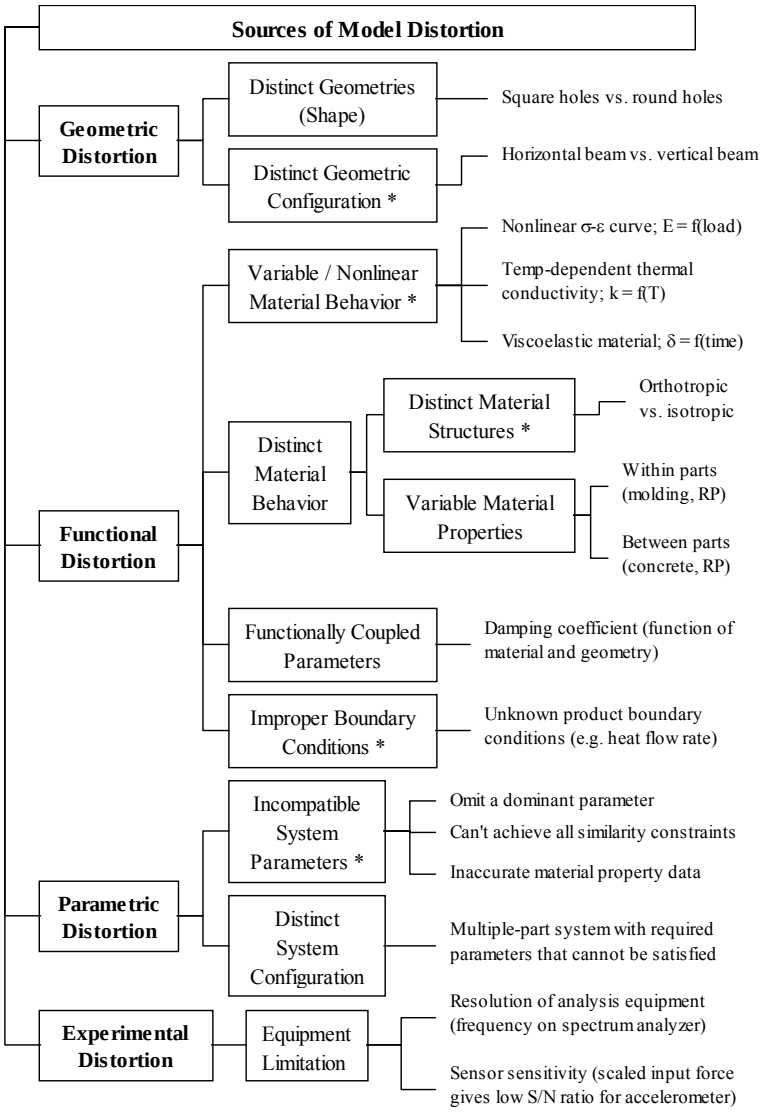

Figure 1. Classification of Model Distortion.

2 Empirical Similitude Method (Concept and Mathematical Foundations)

In an attempt to overcome the inherent difficulties and inaccuracies in the TSM, a new similitude technique known as the *empirical similitude method*, or *ESM*, has been developed (Cho, 1999). The ESM develops a correlation between a model and product empirically, rather through dimensional information alone.

The primary areas of application of the ESM are for systems with the following characteristics:

- The product and model systems are distorted. Product performance can therefore not be predicted accurately through TSM.
- The geometry of the product is such that fabrication and testing of the product directly is difficult. Prediction of product performance through a similitude technique would therefore be beneficial.

- Fabrication of a simplified version of the product (with regard to geometric shape) requires significantly less effort than fabrication of the product itself.

The fundamental concept of the ESM is shown in Fig. 2. Rather than creating just a scale model of the product, as is done in the TSM, the ESM also uses a simplified specimen pair to correlate the behavior of the model and the product. One specimen, called the *model specimen*, is a geometrically simplified version of the model; the other specimen, called the *product specimen*, is a geometrically simplified version of the product. The model specimen is created from the same material and manufacturing process as the model, while the product specimen is created from the same material and manufacturing process as the product.

The concept of the ESM is to create a correlation between distorted systems through empirical testing. The states of the model specimen x_{ms}, the product specimen x_{ps}, and the model x_m, are used to predict the state of the product, x_p. In other words,

$$x_p = f(x_m, x_{ms}, x_{ps}) \tag{4}$$

If the behavior of each system is measured at several different geometric points or at several different loading conditions, then the states must be represented as vectors rather than as single numerical values. By representing vectors in bold type, the above equation is rewritten in vector form as follows:

$$\boldsymbol{x_p} = f(\boldsymbol{x_m}, \boldsymbol{x_{ms}}, \boldsymbol{x_{ps}}) \tag{5}$$

The relationship between any two state vectors can be given, in the most general case, with a fully populated transformation matrix. The theory of the ESM, which relies on the creation and use of such transformation matrices, makes use of the following assumptions (Wood, 2002):

- The model and the model specimen can be tested to determine the state variation caused by changes in geometric shape, or *form.* Since material properties, size, and loading conditions are the same for the model and the model specimen, variations in state between the model and the model specimen are due entirely to the change in geometric shape. A *form transformation matrix F* can be created which represents the variation in the state vector caused by the change in geometric shape.
- The model specimen and the product specimen can be tested to determine the state variation caused by changes in material properties, size, and loading conditions (all of the parameters that are typically scaled between a product and a model). A *scale transformation matrix S* can be created which represents the variation in the state vector caused by changes in size, material properties, and loading conditions, independent of geometric shape. Changes in *size*, in this case, refer to parametric scaling of the overall length dimensions, rather than inherent size changes that accompany changes in shape.
- The transformation matrices *F* and *S* are independent (i.e. there is no coupling between material behavior and geometric shape).

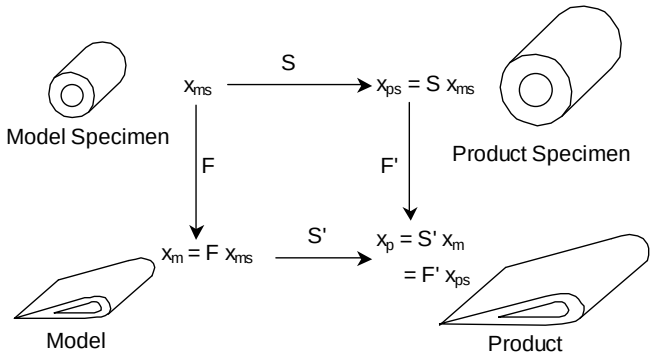

Figure 2. Empirical Similarity Method. Adapted from (Cho, 1999).

By testing the model, the model specimen, and the product specimen, we can extract the transformation matrices *F* and *S* from the following relationships:

$$\begin{aligned} \boldsymbol{x}_{ps} &= \boldsymbol{S}\, \boldsymbol{x}_{ms} \\ \boldsymbol{x}_{m} &= \boldsymbol{F}\, \boldsymbol{x}_{ms} \end{aligned} \tag{6}$$

Since the transformation matrices are considered to be independent, the same scale transformation matrix *S* that relates the model specimen to the product specimen can also be used to relate the model to the product. Likewise, the same form transformation matrix *F* that relates the model specimen to the model can also be used to relate the product specimen to the product. In other words, we assume that *S* = *S'* and *F* = *F'*, as shown in Fig. 2. The state of the product can therefore be predicted by either one of the following equations:

$$\begin{aligned} \boldsymbol{x}_{p} &= \boldsymbol{S}\, \boldsymbol{x}_{m} \\ \boldsymbol{x}_{p} &= \boldsymbol{F}\, \boldsymbol{x}_{ps} \end{aligned} \tag{7}$$

The advantage of the ESM approach over the TSM is that model distortions can be captured in the scale transformation matrix *S*. This approach is contrasted with the TSM which relies solely on dimensional information to correlate systems, with no means of compensating for system distortion. In addition to capturing system distortion, the ESM allows for prediction of product behavior with no *a priori* knowledge about material properties of the product or model systems. The major disadvantage of the ESM is the additional effort required to construct and test the model specimen and product specimen, and calculate the appropriate transformation matrices *S* and *F*.

The position of the ESM in functional testing of products is considered to lie between the TSM and full-scale testing, as shown in Fig. 3. The ESM is presented as a more accurate approach, in general, than the TSM. The ESM is also presented as a better approach for correlating complex systems whose governing parameters may not be well known, as required by the TSM.

Formation of Transformation Matrices

There are three primary approaches for constructing the ESM transformation matrices: pseudo-inverse approach, diagonal matrix approach, and circulant matrix approach. Each approach is presented below.

Pseudo-Inverse Approach

The derivation of the ESM transformation matrices from Eqn. 6 requires that we use the inverse of the

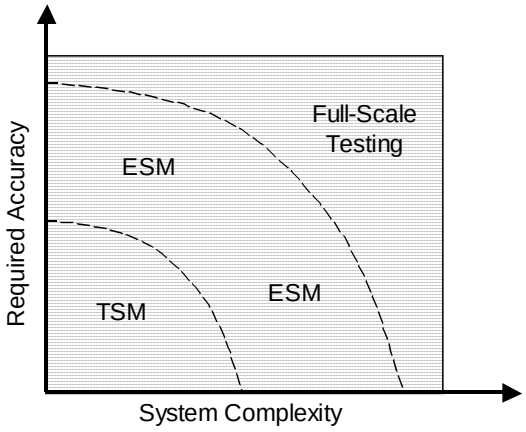

Figure 3. TSM vs. ESM.

model specimen state vector as follows:

$$\boldsymbol{S} = \boldsymbol{x}_{ps}\ \boldsymbol{x}_{ms}^{-1}$$
$$\boldsymbol{F} = \boldsymbol{x}_{m}\ \boldsymbol{x}_{ms}^{-1} \tag{8}$$

However, since $\boldsymbol{x}_{ms}$ is an n x 1 vector rather than an n x n matrix (with n being the number of measurement points taken), we cannot calculate the inverse of $\boldsymbol{x}_{ms}$ directly (recall that we can only take the inverse of a square matrix). One way to circumvent this difficulty is to use the linear algebra concept known as the *pseudo-inverse*.

The pseudo-inverse $\boldsymbol{x}^{+}$ of a vector $\boldsymbol{x}$ is given by the following equation (Strang, 1988):

$$\boldsymbol{x}^{+} = (\boldsymbol{x}^{T}\boldsymbol{x})^{-1}\boldsymbol{x}^{T} \tag{9}$$

By using the pseudo-inverse of $\boldsymbol{x}_{ms}$, the transformation matrices *S* and *F* can be derived as follows:

$$\boldsymbol{S} = \boldsymbol{x}_{ps}\,\boldsymbol{x}_{ms}^{+}$$
$$\boldsymbol{F} = \boldsymbol{x}_{m}\,\boldsymbol{x}_{ms}^{+} \tag{10}$$

The pseudo-inverse solution shown in Eqn. 10 represents the *least squares solution* to the over determined system represented by Eqn. 6. We note from Fig. 2, however, that the two ESM paths for predicting the state of the product should be identical (i.e. assuming that $\mathbf{S} = \mathbf{S'}$ and $\mathbf{F} = \mathbf{F'}$, $\mathbf{x_p} = \mathbf{SFx_{ms}}$ or $\mathbf{x_p} = \mathbf{FSx_{ms}}$). This assumption of the ESM requires that $\mathbf{SF} = \mathbf{FS}$. Since the pseudo-inverse approach produces fully populated matrices that are not, in general, commutative under matrix multiplication, the basic assumption of the ESM that $\mathbf{SF} = \mathbf{FS}$ is violated when the pseudo-inverse technique is used in deriving the transformation matrices. We look therefore, for alternative approaches to deriving ESM transformation matrices that satisfy the basic assumption that $\mathbf{SF} = \mathbf{FS}$.

Diagonal Matrix Approach

The concept behind the diagonal matrix approach is that the value of each entry in a state vector is dependent *only on the value of the corresponding entry* of the related state vector. For example, consider the system $\boldsymbol{x}_{ps} = \boldsymbol{S}\boldsymbol{x}_{ms}$ where each state vector has three entries (i.e. the vectors have a dimension of 3). In the general case, **S** is a fully populated matrix, and the system is represented as

$$\begin{bmatrix} x_{ps,1} \\ x_{ps,2} \\ x_{ps,3} \end{bmatrix} = \begin{bmatrix} s_{11} & s_{12} & s_{13} \\ s_{21} & s_{22} & s_{23} \\ s_{31} & s_{32} & s_{33} \end{bmatrix} \begin{bmatrix} x_{ms,1} \\ x_{ms,2} \\ x_{ms,3} \end{bmatrix}. \tag{11}$$

We see in Eqn. 11 that $\mathbf{x_{ps,1}}$, for example, is not determined just from $\mathbf{x_{ms,1}}$; rather, it is calculated as a linear combination of $\mathbf{x_{ms,1}}$, $\mathbf{x_{ms,2}}$, and $\mathbf{x_{ms,3}}$. If we assume, however, that each entry of $\mathbf{x_{ps}}$ can be determined entirely from the corresponding entry of $\mathbf{x_{ms}}$, we can modify Eqn. 11 to take the following form:

$$\begin{bmatrix} x_{ps,1} \\ x_{ps,2} \\ x_{ps,3} \end{bmatrix} = \begin{bmatrix} s_{11} & 0 & 0 \\ 0 & s_{22} & 0 \\ 0 & 0 & s_{33} \end{bmatrix} \begin{bmatrix} x_{ms,1} \\ x_{ms,2} \\ x_{ms,3} \end{bmatrix}. \tag{12}$$

We now have

$$x_{ps,1} = s_{11}x_{ms,1}$$
$$x_{ps,2} = s_{22}x_{ms,2} \tag{13}$$
$$x_{ps,3} = s_{33}x_{ms,3}$$

where each point in the product specimen is simply a scaled value of the corresponding point in the model specimen.

When the transformation matrix **S** is diagonal, as in Eqn. 12, the procedure for calculating **S** given $\mathbf{x_{ps}}$ and $\mathbf{x_{ms}}$ is much more straightforward than it is with the pseudo-inverse approach. For the diagonal case, each line in Eqn. 13 is simply solved for the respective scale factor s_{ii}, as follows:

$$\begin{aligned} s_{11} &= x_{ps,1} / x_{ms,1} \\ s_{22} &= x_{ps,2} / x_{ms,2} \\ s_{33} &= x_{ps,3} / x_{ms,3} \end{aligned} \tag{14}$$

Each scale factor is then placed in the appropriate location along the diagonal, and the transformation matrix **S** is complete!

It is important to emphasize the relationship between this ESM diagonal method and the TSM method, and to point out the valuable insight about model distortion that can be obtained with the diagonal method. Suppose that scale factors are calculated according to Eqn. 14 and that *they are all the same*; this situation represents a well-scaled system (the degree of model distortion is zero). Now suppose that scale factors are calculated for a different system according to Eqn. 14 and that *they have different values*; this situation represents a system with model distortions (the degree of model distortion is characterized by the variation in the scale factors). Recall that the need for the ESM arises from distorted systems for which a constant scale factor fails to accurately correlate the two systems; the entries of the diagonal matrix show how the scale factor changes as you move from point to point within the system (a *point* in this case can represent a physical location in the system, a specific loading condition, or any other independent variable for which one is measuring system behavior).

Another important aspect of the diagonal matrix approach is that the ESM requirement that **SF** = **FS** is always satisfied. The fact that diagonal matrices are always commutative for matrix multiplication can be illustrated with the following example:

$$\begin{bmatrix} a_{11} & 0 \\ 0 & a_{22} \end{bmatrix}\begin{bmatrix} b_{11} & 0 \\ 0 & b_{22} \end{bmatrix} = \begin{bmatrix} b_{11} & 0 \\ 0 & b_{22} \end{bmatrix}\begin{bmatrix} a_{11} & 0 \\ 0 & a_{22} \end{bmatrix} = \begin{bmatrix} a_{11}b_{11} & 0 \\ 0 & a_{22}b_{22} \end{bmatrix} \tag{15}$$

Eqn. 15 can easily be extended to *n* dimensions.

Circulant Matrix Approach

The final method for constructing ESM transformation matrices uses the circulant matrix technique. Transforming a vector into a circulant matrix can be thought of as a matrix manipulation, similar to taking the transpose of a matrix. The circulant form of a vector is constructed as follows:

$$x = \begin{bmatrix} x_1 \\ x_2 \\ \vdots \\ x_n \end{bmatrix} \quad \Rightarrow \quad cir(x) = \begin{bmatrix} x_1 & x_n & \cdots & x_2 \\ x_2 & x_1 & \cdots & x_3 \\ \vdots & \vdots & & \vdots \\ x_n & x_{n-1} & \cdots & x_1 \end{bmatrix} \tag{16}$$

By using the circulant form of each state vector, the basic ESM relationships shown in Eqn. 6 become

$$\begin{aligned} cir(\mathbf{x_{ps}}) &= \mathbf{S}\ cir(\mathbf{x_{ms}}) \\ cir(\mathbf{x_m}) &= \mathbf{F}\ cir(\mathbf{x_{ms}}) \end{aligned} \tag{17}$$

Since a circulant matrix is square by definition, the inverse of cir($\mathbf{x_{ms}}$) can be calculated (provided it's columns are linearly independent) and multiplied to both sides of Eqn. 17 to give

$$\boldsymbol{S} = cir(\boldsymbol{x}_{ps})\, cir(\boldsymbol{x}_{ms})^{-1}$$
$$\boldsymbol{F} = cir(\boldsymbol{x}_{m})\, cir(\boldsymbol{x}_{ms})^{-1} \quad (18)$$

Since the inverse of a circulant matrix is also a circulant matrix, and the product of two circulant matrices is also a circulant matrix (Davis, 1979), we conclude that Eqn. 18 produces *circulant* transformation matrices **S** and **F**. The fact that **S** and **F** are circulant is an important conclusion since *circulant matrices also commute under matrix multiplication* (Davis, 1979). This means that **SF** = **FS** as required by the ESM.

3 Applications – Cantilever Beams

In order to illustrate the improvement of the ESM over the TSM for distorted systems, we consider the problem of predicting the deflection of a cantilever beam under a concentrated load at the tip. Finite element analysis is used to model the deflection of the beams. The product and model beams have five holes along their length. The product beam is modeled with linear material properties (a linear stress-strain curve, representing a constant value of Young's modulus) and the model beam is modeled with nonlinear material properties (a nonlinear stress-strain curve, representing a variable value of Young's modulus). Since the model material is nonlinear while the product material is linear, the system is distorted and the TSM is expected to yield inaccurate results. The deflection of the product beam is predicted using both the TSM and the ESM in order to compare results from the two approaches. The ESM setup is shown in Fig. 4.

The nonlinear stress-strain behavior of the model system is defined with a Ramberg-Osgood curve, which is described by the following equation (ABAQUS, 2001):

$$\varepsilon = \frac{\sigma}{E}\left(1 + \alpha\left(\frac{\sigma}{\sigma^0}\right)^{n-1}\right) \quad (19)$$

where σ = stress
ε = strain
E = Young's modulus (defined as the slope of the stress-strain curve at zero stress)
α = "yield" offset
σ^0 = yield stress in the sense that, when $\sigma = \sigma^0$, $\varepsilon = ((1+\alpha)\sigma^0)/E$
n = hardening exponent for the "plastic" (nonlinear) term: $n > 1$

By varying the parameters in the Ramberg-Osgood equation, three different material properties that exhibit increasing degrees of nonlinearity are defined. The parameters used to define these material properties are

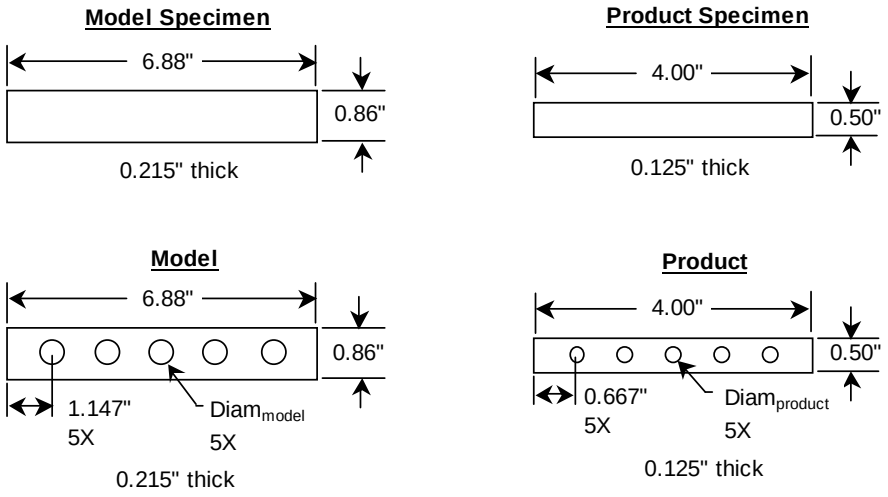

Figure 4. Setup for ESM Study 1.

shown in Table 1, and the resultant stress-strain curves are shown in Fig. 5. The straight lines in Fig. 5 represent the slopes of the stress-strain curves at zero stress (given by E in Table 1), which is the traditional definition of Young's modulus for a nonlinear stress-strain curve. The three curves shown in Fig. 5 represent three different material property cases for the model and the model specimen in this study. The product and product specimen maintain a linear stress-strain relationship, with a Young's modulus of 10,150 ksi (equal to that of aluminum).

Table 1. Parameters for Ramberg-Osgood curve.

	E (ksi)	α	σ^0 (ksi)	n
Material 1	150	0.40	3	2.0
Material 2	320	0.43	3	3.0
Material 3	500	2.00	3	2.5

The "degree of nonlinearity" in the stress-strain curves (which represents the "degree of model distortion") can be quantified through a residual sum of squares between the points that define the linear curves and those that define the corresponding nonlinear curves (DeVor, 1992). Each linear curve in Fig. 5 is defined by calculating strain at every 10 psi increment of stress using the linear relationship $\varepsilon = \sigma / E$. Each corresponding nonlinear curve in Fig. 5 is defined by calculating strain at every 10 psi increment of stress using Eqn. 19. The residual sum of squares is then calculated as follows:

$$SS(residual) = \sum_{i=1}^{n} (\varepsilon_{nl} - \varepsilon_{l})^2 \tag{20}$$

where ε_{nl} is the nonlinear value of strain at each increment of stress, ε_{l} is the linear value of strain at each increment of stress, and n is the total number of stress increments. Table 2 shows the calculated residual sum of squares for each nonlinear stress-strain curve in Fig. 5. The values in Table 2 indicate that each successive material exhibits a higher degree of nonlinearity, which signifies that each successive material represents a higher degree of model distortion.

Three different geometric cases are also considered in this study. The geometry of the model, product, model specimen, and product specimen are shown in Fig. 4. The three different geometric cases involve different sizes of holes in the product (and, correspondingly, in the model). The three hole sizes considered in the study are shown in Table 3. Notice that a constant scale factor of 0.5814 relates all geometric features of the model to the product. The only distortion between the model family and the product family is in the value and behavior of Young's modulus.

A total of nine cases have now been defined for the study (three different hole sizes for each of the three different material properties). The goal of the study is to determine the influence that changes in geometric shape and changes in model distortion have on TSM and ESM results. In each case a load of 20 lbs is applied

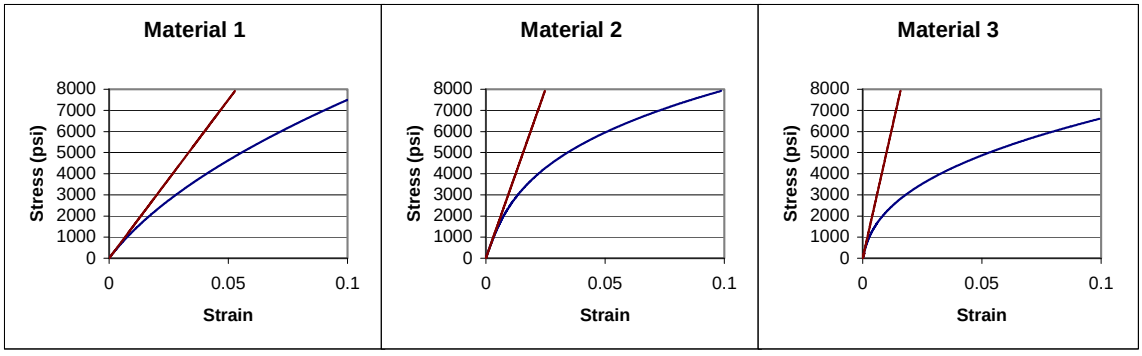

Figure 5. Nonlinear Stress-Strain Curves for ESM Study 1.

Table 2. Residual Sum of Squares for Model Materials.

	Range of Stress (psi)	**SS(residual)**
Material 1	0 - 8000	0.52
Material 2	0 - 8000	0.67
Material 3	0 - 8000	2.60

Table 3. Three Geometric Cases for ESM Study 1.

	$Diam_{product}$ (in)	**$Diam_{model}$ (in)**
Geometry 1	0.150	0.258
Geometry 2	0.250	0.430
Geometry 3	0.350	0.602

to one end of the product beam while the other end of the beam is held fixed. (The required load for the model beam is determined from TSM scale factors assuming a constant value for Young's modulus). The deflection of the tip of the beam, which is recorded at ten equal load increments (at 2 lbs, 4 lbs, 6 lbs, … 20 lbs), represents the *state vector* for each beam. The transformation matrix is derived using both the pseudo-inverse (*pi*) approach and the circulant matrix (*cir*) approaches. The ESM technique is then used to predict the state of the product. The errors in the TSM and ESM approaches are determined by comparing predicted values with the actual state of the product.

The average errors from the TSM, ESM pseudo-inverse (*pi*), and ESM circulant matrix (*cir*) approaches for all nine cases are compiled in Table 4. A review of the table shows that, for any given material, prediction errors increase as the change in geometric shape increases (with Geometry 1 having the least change and Geometry 3 having the greatest). Likewise, for any given geometric shape, prediction errors tend to increase as the degree of material distortion increases (with Material 1 having the least distortion and Material 3 having the greatest). The only exceptions to this trend, which are due to the fact that the model distortion for Material 2 is actually smaller than that for Material 1 at low values of stress, are highlighted with an asterisk. Note that, in every case, the ESM predictions produce less error than the TSM prediction.

Fig. 6 contains a plot of ESM error as a function of model distortion (we assume zero prediction error for zero model distortion in this case). Recall that model distortion in this case is represented by the residual sum of squares of the nonlinear stress-strain curves for the various materials, as shown in Table 2. The plot in Fig. 6 reflects the results obtained from the circulant matrix approach, although TSM or ESM pseudo-inverse results show similar trends. The results shown in Fig. 6 lead to the same conclusions that can be drawn from Table 4 - that prediction error tends to increase with increased changes in geometric shape and with increased levels of model distortion.

Table 4. Average Errors from Various Similitude Approaches.

	Geometry 1		Geometry 2		Geometry 3	
Material 1	TSM	4.06 %	TSM	4.86 %	TSM	6.26 %
	ESM_{pi}	0.53 %	ESM_{pi}	1.31 %	ESM_{pi}	2.41 %
	ESM_{cir}	0.54 %	ESM_{cir}	1.31 %	ESM_{cir}	2.64 %
Material 2	TSM *	2.79 %	TSM *	4.20 %	TSM	7.94 %
	ESM_{pi}	0.67 %	ESM_{pi}	2.50 %	ESM_{pi}	7.62 %
	ESM_{cir} *	0.52 %	ESM_{cir}	1.90 %	ESM_{cir}	5.54 %
Material 3	TSM	36.48 %	TSM	45.88 %	TSM	67.66 %
	ESM_{pi}	3.44 %	ESM_{pi}	11.89 %	ESM_{pi}	28.00 %
	ESM_{cir}	2.88 %	ESM_{cir}	10.10 %	ESM_{cir}	26.88 %

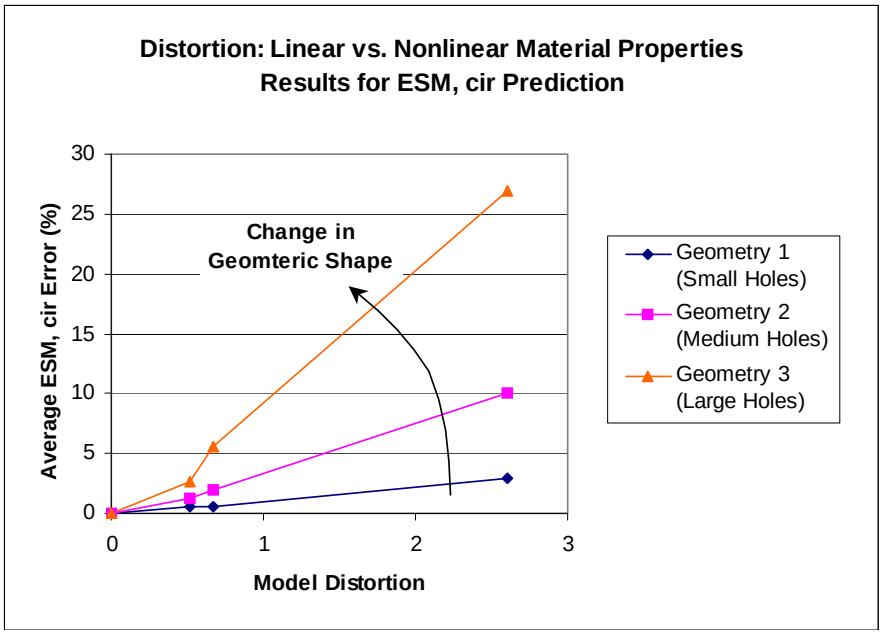

Figure 6. Prediction Error vs. Model Distortion for ESM Study 1.

4 Specimen Distortions and the Advanced Similitude Technique

Application of the current ESM is valid for situations in which **S = S'** and **F = F'**. Conditions which cause **S ≠ S'** or **F ≠ F'** are referred to as *specimen distortions* since they involve inconsistencies between the product / model system and the specimen pair. This type of distortion is in contrast to *model distortions* presented earlier, which refer to inconsistent scaling between a model and a product. Since specimen distortions cause **S ≠ S'** or **F ≠ F',** they cause the ESM theory to be violated and produce errors in ESM predictions. Several sources of specimen distortion are illustrated in Fig. 7, along with specific examples of each type of distortion.

In order to clarify the underlying theory of the ESM, the two-dimensional illustration of the ESM, as shown in Fig. 2, is converted to a three-dimensional illustration, as shown in Fig. 8. In Fig. 8, a description of material properties, size, and loading conditions is plotted on the x-axis, a description of geometric shape is plotted on the y-axis, and the system response is plotted on the z-axis. (Note that $[S]_1$ and $[F]_1$ in Fig. 8 represents S' and F', respectively, in Fig. 2). The four configurations shown in Fig. 8 correspond to the traditional ESM systems (viz. product, product specimen, model, and model specimen). Although the system response is shown as a single point in the figure, the response can more generally be represented as a vector. Fig. 8 illustrates that, for the most general case, the transformation matrices that relate the four system states are all different.

The goal of the advanced ESM is to capture the change in the *Scale* transformation matrix as the *Form* parameters change or, equivalently, to capture the change in the *Form* transformation matrix as the *Scale* parameters change. An intermediate specimen pair is presented as a means of capturing the variation in the transformation matrices, as illustrated in Fig. 9. By defining an intermediate specimen pair that lies between the original system pairs, the variation in the transformation matrix that occurs from one specimen pair to the next can be extrapolated to predict the transformation matrix between the model and the product. (An alternate approach is to define the additional specimen pair *outside* of the original system pairs and *interpolate* to predict the transformation matrix between the model and the product). The decision of whether

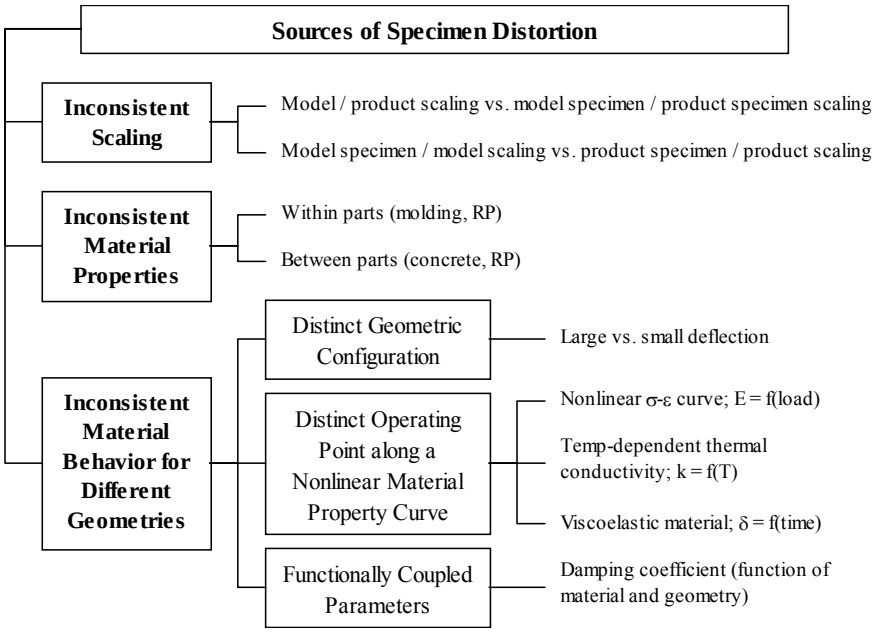

Figure 7. Sources of Specimen Distortion.

to capture changes in the *Scale* transformation matrix or the *Form* transformation matrix depends on whether it is easier to characterize changes in geometric shape for a particular problem or to characterize changes in material properties, size, and loading conditions.

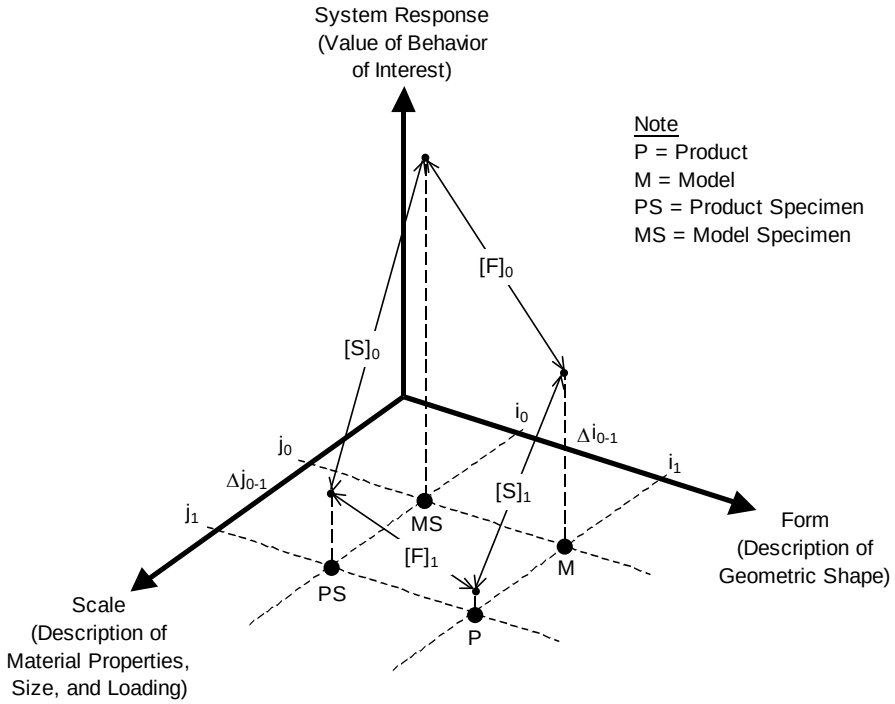

Figure 8. Illustration of Empirical Similarity Method.

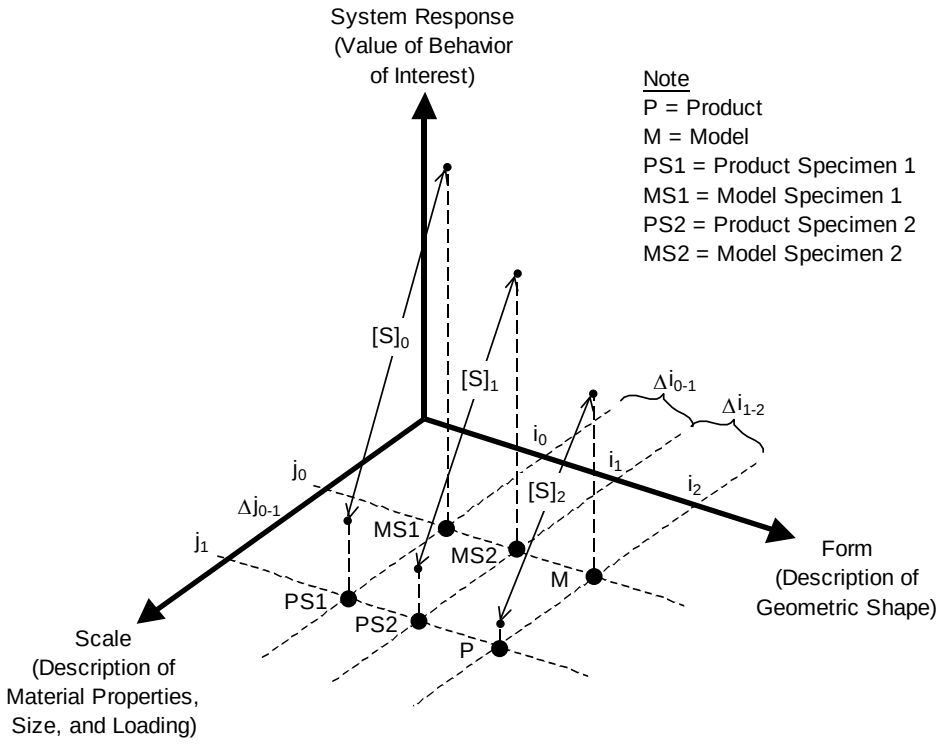

Figure 9. Illustration of Advanced Empirical Similarity Method.

In the advanced ESM, each transformation matrix signifies a "data point," and an interpolating polynomial is constructed to describe the trend in the data. For a single intermediate specimen pair, a first order polynomial is constructed; for two intermediate specimen pairs, a second order polynomial is constructed; etc. In general, *n* intermediate specimen pairs allow for the construction of an n^{th} order polynomial.

The polynomial used in the advanced similitude method, which is a Lagrange polynomial that incorporates divided differences, is known as *Newton's interpolatory divided-difference formula* and is given as follows (Burden, 1989):

$$P_n(x) = f\{x_0\} + \sum_{k=1}^{n} f\{x_0, x_1, \cdots, x_k\}(x - x_0)\cdots(x - x_{k-1}). \tag{21}$$

where the notation *f{x}* is the *divided-difference notation*. When applying the interpolatory polynomial in Eqn. 21 to the ESM, the points x_m represent either increments in *form* (i_0, i_1, …) or increments in *scale* (j_0, j_1, …), depending on the dimension in Fig. 9 that is being discretized, and the value of the function $f(x_m)$ represents the transformation matrix at the specified point. For example, if the *form* dimension is being discretized, as shown in Fig. 9, the first divided difference is

$$S\{i_0, i_1\} = \frac{[S]_1 - [S]_0}{i_1 - i_0} \tag{22}$$

and the first order polynomial prediction of $[S]_2$ becomes

$$[S]_{2,1stOrder} = [S]_0 + S\{i_0, i_1\}(i_2 - i_0) \tag{23}$$

which, in this case, is simply a linear extrapolation. This approach can be extended to higher order polynomials, as described in Eqn. 21, according to the number of intermediate specimen pairs that are available. Higher order polynomials generally lead to more accurate predictions of the transformation matrix.

5 Application of the Advanced Similitude Technique

The advanced ESM technique is now applied to the cantilever beam problem presented earlier. The beam with large holes is considered to be the product beam, and the other beams are used as intermediate specimen pairs. The Advanced ESM setup is shown in Fig. 10. With two intermediate specimen pairs, both 1st order and 2nd order polynomial approximations to $\mathbf{S_3}$ can be computed.

The first step in the advanced ESM technique is to compute the necessary divided differences, as described by Eqn. 22. The matrix difference shown in Eqn. 22 is calculated by subtracting corresponding entries from each respective matrix. The step size shown in Eqn. 22 ($i_1 - i_0$) is, in this case, simply the difference in hole sizes.

With the divided differences computed, the transformation matrix between the product and the model ($\mathbf{S_3}$, as shown in Fig. 10) is now calculated using Eqn. 21. Both first and second order polynomial predictions of $\mathbf{S_3}$ are calculated. The improvement in the ESM results obtained from using the "corrected" transformation matrix is shown in Fig. 11.

The results from the advanced ESM study show significant reductions in prediction error when a corrected transformation matrix is used. Although Fig. 11 shows results obtained from the circulant matrix approach, the diagonal matrix results show similar trends. The figure confirms that higher order polynomials produce more accurate predictions of the desired transformation matrix and, consequently, less prediction error.

6 Heat Sink Application

Proper control of the steady state temperature of CPU surfaces is critical to CPU performance. For example, Intel recommends that the center of the Pentium II CPU processor be kept below 65 °C. The surface of the Pentium II processor can reach up to 150 °C without cooling. In addition, an advanced chip mounting technology (single edge connector) has been employed for more compact component mounting in which the mass of the CPU and its cooling system should be less than 105 *g* (Intel, 1998). The requirement for effective heat dissipation, coupled with the constraint that the overall system mass must be 105 *g* or less, makes the design of CPU heat sinks a challenging problem.

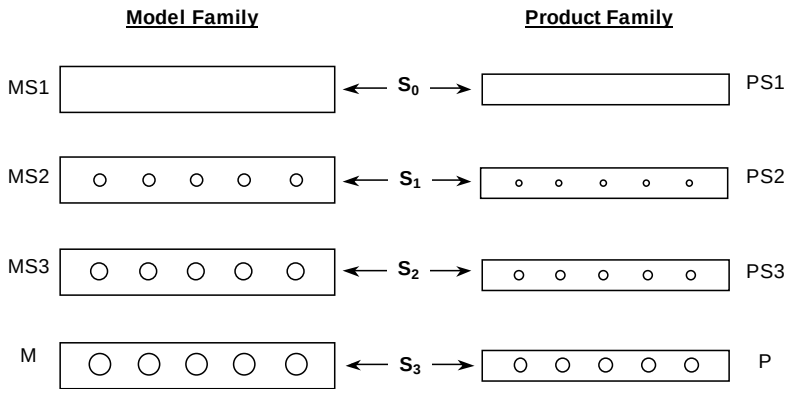

Figure 10. Application of Advanced Empirical Similarity Method.

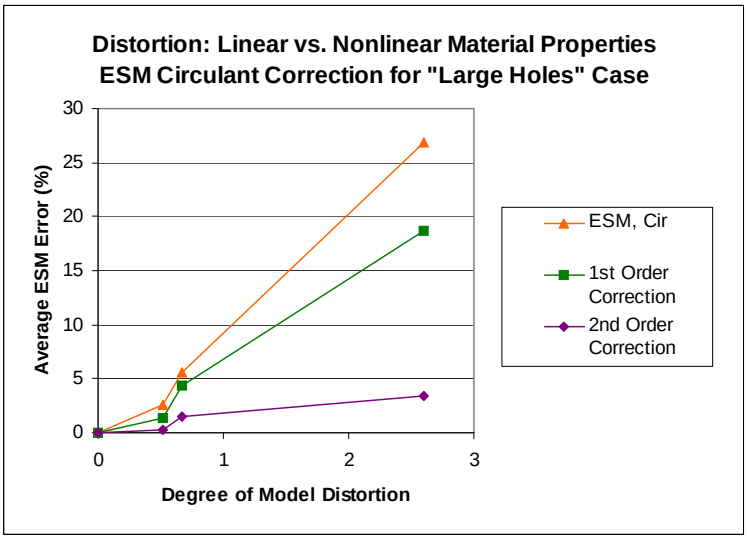

Figure 11. Reduction in Average Error for ESM Study 1.

Virtual modeling of the steady-state temperature of thermal systems, which are composed of a CPU, a heat sink, and a cooling fan to circulate heated air, still needs improvement (Nadworny 1995, Fisher 1997). Virtual modeling of the CPU cooling process requires complex computational fluid dynamics (CFD). One problem in CFD modeling is the fact that including detailed geometry creates a model of unmanageable size (Linton, 1995). In this subsection, we examine the feasibility of performing CPU cooling tests with polymer heat sinks fabricated with a rapid prototyping technique called selective laser sintering (SLS) (Beaman et. al., 1997; Conley, 1997; Jacobs, 1992). The heat sinks were produced from DuraForm (a polyamide-based powder for selective laser sintering processes). Results of the tests are used with the ESM to predict the performance of the actual heat sink product.

Once again we begin the ESM with a lumped model of the system. A CPU cooling process can be approximated as an electric circuit (Incropera, 1981; Kline, 1965). The lumped model of the CPU cooling process with heat sinks is depicted in Fig. 12. In the figure, h and k are unknown effective thermal convection and conduction coefficients, while A and A_c denote the effective convection and conduction areas of heat sinks, respectively. A resistor array is used to represent the CPU. The lumped model is built with the assumptions that (1) heat transfer from the sides and the bottom surface of the heat source (i.e. CPU) is negligible, (2) the contact thermal resistance is negligible, and (3) the thermal conductivity is not dependent on temperature. It should be noted that, although the heat sink cooling process appears at first glance to be a single material problem, the phenomenon is affected by two main physical components, viz. the thermal boundary layer and the heat sink. Hence the lumped ESM is used to predict product performance.
From Fig. 10 and the above assumptions, the surface temperature of the resistor array with the generic DuraForm heat sink (model specimen) can be represented as

$$T_{ms} = q_m (R_h + R_k) + T_\infty \tag{24}$$

where $R_h = \frac{1}{hA}$ and $R_k = \frac{L}{kA_c}$ are unknown convection and conduction thermal resistances, respectively, q is the unknown heat transfer rate, and $T_\infty = 19°$ C is the ambient temperature. The temperature of the model, product specimen, and product can now be represented as

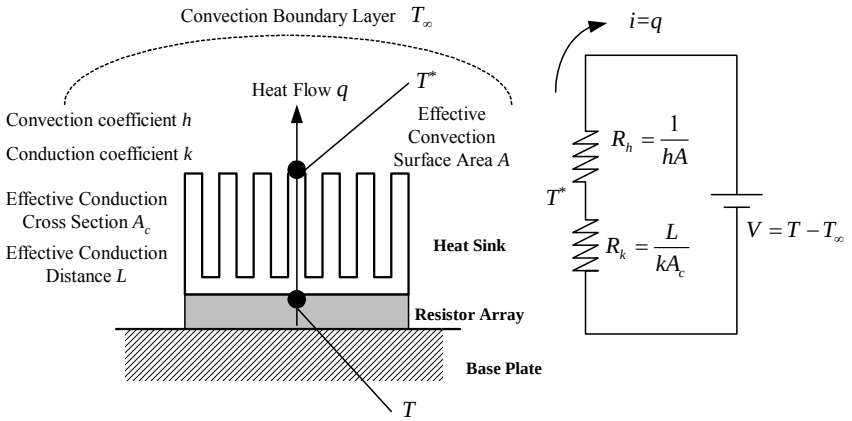

Figure 12: Lumped Model and Equivalent Electric Circuit of Heat Sink Systems

$$\begin{aligned} T_m &= q_m(\phi_h R_h + \phi_k R_k) + T_\infty \\ T_{ps} &= q_p(\lambda_h R_h + \lambda_k R_k) + T_\infty \\ T_p &= q_p(\phi_k \lambda_h R_h + \phi_k \lambda_k R_k) + T_\infty . \end{aligned} \tag{25}$$

In Eqn. (25), λ_h and λ_k are scale factors that represent the variation of R_h and R_k under material and boundary condition changes (with no change in the heat sink geometry). In contrast, ϕ_h and ϕ_k are form factors that represent the variation of R_h and R_k under purely geometry changes.

More information is needed to represent T_p for the heat sink as a function of T_m, T_{ms}, T_{ps} since the number of unknowns (T_p, ϕ_h, ϕ_k, λ_h, λ_k, R_h, R_k) exceeds the number of given equations. In this example, we measure T* (the temperature at the top of the heat sink, as shown in Fig. 10) experimentally to estimate T_p from T_m, T_{ms}, T_{ps}, T_m*, T_{ms}*, and T_{ps}*.

By sub-modeling the convection process, the following equations can be derived:

$$T_{ms}^* - T_\infty = q_m R_h, \quad T_m^* - T_\infty = q_m \phi_h R_h, \quad T_{ps}^* - T_\infty = q_p \lambda_h R_h, \tag{26}$$

Similarly, by focusing on the conduction process, the following equations can be derived:

$$T_{ms} - T_{ms}^* = q_m R_k, \quad T_m - T_m^* = q_m \phi_k R_k, \quad T_{ps} - T_{ps}^* = q_p \lambda_k R_k \tag{27}$$

From the above six additional equations, the following unknown form factors can be derived.

$$\phi_h = \frac{T_m^* - T_\infty}{T_{ms}^* - T_\infty}, \quad \phi_k = \frac{T_m - T_m^*}{T_{ms} - T_{ms}^*}. \tag{28}$$

Substituting Eqns. (26), (27), and (28) into the last of Eqn. (25) gives the ESM prediction equation for the heat sink as

$$T_p = (T_{ps}^* - T_\infty)\left(\frac{T_m^* - T_\infty}{T_{ms}^* - T_\infty}\right) + (T_{ps} - T_{ps}^*)\left(\frac{T_m - T_m^*}{T_{ms} - T_{ms}^*}\right) + T_\infty . \tag{29}$$

In order to predict the temperature of the aluminum CPU heat sink, as described in Eqn. (29), a model and model specimen were created, and a product specimen was selected. The heat sinks used in this experiment are shown in Fig. 13. First, the aluminum CPU heat sink (with complex geometry) was established as the final product of interest. A generic aluminum heat sink (i.e. a previous version of the

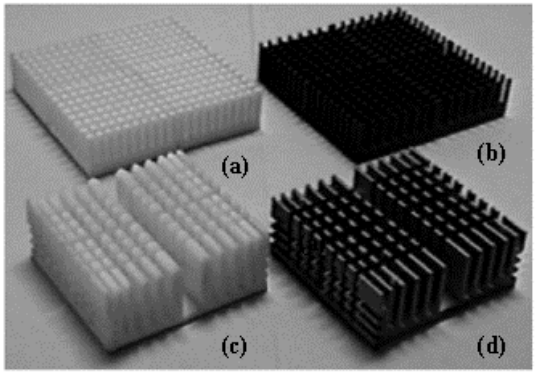

(a) Top Left: Durafom Generic Heat Sink (Model Specimen)
(b) Top Right: Aluminum Generic Heat Sink (Product Specimen)
(c) Bottom Left: Durafom Pentium Heat Sink (Model)
(d) Bottom Right: Aluminum Pentium Heat Sink (Product)

Figure 13: DuraForm and Aluminum Heat Sinks

product with relatively simple geometry) was then selected as the product specimen. Model heat sinks were then fabricated using DuraForm in the SLS process.

Detailed top views of the targets (aluminum and DuraForm CPU heat sinks) and specimens (aluminum and DuraForm generic heat sinks) and the six chosen measurement locations are shown in Fig. 14. A resistor array composed of four power resistors was used to emulate the CPU. Fig. 15 depicts the overall view of the

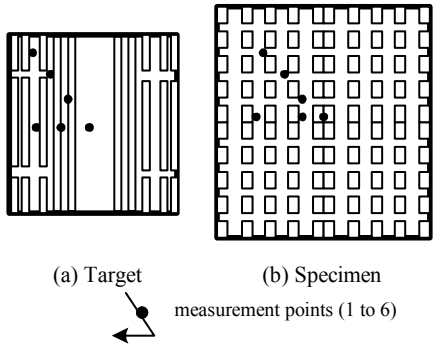

Figure 14: Top View of Heat Sinks

Figure 15: Overview of CPU Cooling Experiment

Table 5. Model and Product Systems for CPU Cooling Test

Test Conditions	Model System	Product System
Resistor Voltage (V_r)	15V	20V
Cooling Fan Voltage (V_f)	20V	15V
Heat Sink Material	DuraForm	Aluminum
Temperature at Heat Sink Top	$T_m^* = 54°\text{C}, \text{T}_{\text{ms}}^* = 65°C$	$T_{ps}^* = 25°C$

experiment. Initially the same voltage was supplied to the resistor array for both the DuraForm and the aluminum heat sinks. However, the temperature of the resistor surface rose too high for the DuraForm heat sinks. In order to prevent thermal deformation when testing with DuraForm heat sinks, the resistor voltage was lowered and the fan voltage (and thus, fan speed) was increased for better heat dissipation. Thus the boundary conditions, as well as the material properties, were scaled for the heat sink models. Table 5 shows the system parameter settings for the experiment along with the steady-state temperature at the top of the heat sink.

Fig. 16 shows the measured steady-state temperature at the six selected points of the resistor surface with both DuraForm and aluminum heat sinks. The generic aluminum heat sink shows better cooling performance (due to its larger size) than the aluminum CPU heat sink. The DuraForm heat sinks increased the surface temperature by working as heat insulators rather than conductors. It is interesting to note the opposite trends in the two plots: the generic aluminum heat sink is the better conductor, and the DuraForm version of the generic heat sink is the better insulator. One can perceive the difficulty in traditional scale testing with such qualitative dissimilarity.

The temperatures at the six points of the resistor array surface with the aluminum CPU heat sink are predicted by using Eqn. (29) and the measurements shown in Table 5 and Fig. 16. The measured temperature of the resistor array surface with the aluminum CPU heat sink is used to verify the predicted results. Fig. 17 compares the predicted and actual temperatures of the resistor array surface with the aluminum CPU heat sink. The prediction error is within 2 °C overall. The testing results demonstrate the accuracy of the lumped ESM.

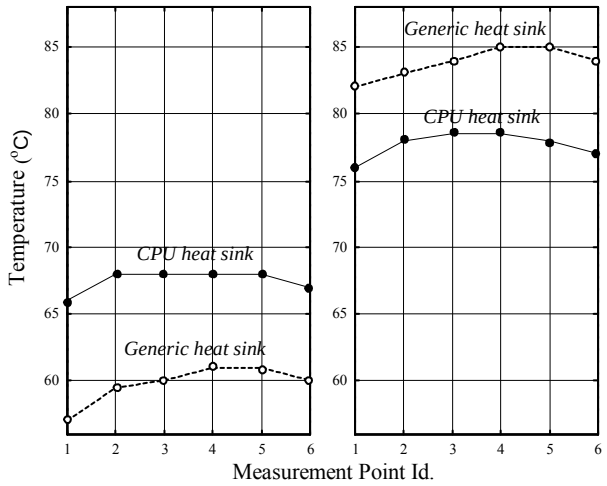

(a) With Aluminium Heat Sinks (b) With DuraForm Heat Sinks

Figure 16: Measured Surface Temperature

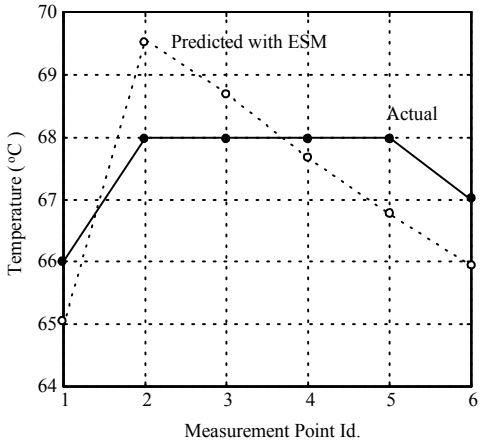

Figure 17: Predicted Surface temperature

It is worthwhile to note that the temperature of the CPU (resistor array) surface with the aluminum heat sink was predicted with the ESM without knowing such system parameters as thermal conductivity or convection coefficients explicitly. The TSM, on the other hand, requires *a priori* knowledge of such parameters in order to develop proper scaling factors. Due to the distinctive thermal conductivity and heat capacitance of DuraForm and aluminum relative to air, even qualitative temperature prediction is difficult. Through the new lumped ESM, however, we successfully correlated the steady-state thermal behavior of heat sink systems with highly distorted configurations.

7 Conclusions

The concept of the ESM involves deriving similarity transformations by employing a specimen pair. The ESM can be used for a wide array of problems, but is especially suited for products that have geometric or material requirements that result in high fabrication costs. The ESM is also well suited for products for which a product specimen already exists (such as in product redesign) or for which the product specimen can be easily fabricated.

Application of the ESM also has certain limitations. For example, an implicit requirement of the ESM is that geometric simplifications used for the specimen pair, as well as material changes used in the models, must not alter the overall functional behavior of the product (e.g. electromagnetic characteristics of a product cannot be predicted with a Duraform model since Duraform does not conduct electricity). This inherent condition of the ESM requires a basic knowledge of the effect of various system parameters on product performance, although it is still much less than that needed for the TSM. In addition, the lumped ESM requires that appropriate lumped models can be created for the system of interest. The creation of an appropriate lumped model may be difficult in some cases. Care should be taken when creating lumped models to include such effects as contact thermal resistances when necessary. Various spatio-temporal measurement points may be used to validate modeling assumptions.

Acknowledgments

The research reported in this document was supported, in part, by NSF grant number DMI-9988880 and ATP grant number 003658-0079-2001. The authors also wish to acknowledge the support of the Cullen Trust for Higher Education Endowed Professorship in Engineering #1. Any opinions, findings, or recommendations are those of the authors and do not necessarily reflect the views of the sponsors.

REFERENCES

ABAQUS/Standard User's Manual, Version 6.2, 2001, Hibbitt, Karlsson & Sorensen, Inc.

Baker, W.E., Westine, P.S., Dodge, F.T. 1991. Similarity Methods and Engineering Dynamics: Theory and Practice of Scale Modeling, Elsevier.
Beaman, J. J. et al. 1997. *Solid Freeform Fabrication: A new Direction in Manufacturing*, Kluwer, Norwell.
Bluman, G.W., Kumei, S. 1989. *Symmetries and Differential Equations*, Springer-Verlag, New York.
Bridgman, P.W. 1937. *Dimensional Analysis*, Yale University Press, New Haven.
Burden, R. L., and Faires, J. D., 1989, Numerical Analysis, PWS Kent, Boston.
Cho, U., 1999, Novel Empirical Similarity Method for Rapid Product Testing and Development, Doctoral dissertation, The University of Texas at Austin.
Cho, U., Wood, K.L., and Crawford, R.H. 1998(a) ``Online Functional Test with Rapid Prototypes: A Novel Empirical Similarity Method," Rapid Prototyping Journal, Vol. 4, Number 3, pp.128-138.
Cho, U., Wood, K.L., and Crawford, R.H. 1998(b) ``Novel Empirical Similarity Method for the Reliable Product Test with Rapid Prototypes," In *Proceedings of the 1998 ASME DETC*, number 98-DETC/DAC-5605, Atlanta, GA. ASME.
Cho, U., Wood, K.L., and Crawford, R.H. 1999 ``Error Measures for Functional Product Testing," In *Proceedings of the 1999 ASME DETC*, number 99-DETC/DFM-8913, Las Vegas, NV. ASME.
Conley, J. G., and Marcus, H. L. 1997. "Rapid Prototyping and Solid Free Form Fabrication," *Journal of Manufacturing Science and Engineering*, Vol. 119, pp. 811-816.
Davis, P. J., 1979, Circulant Matrices, John Wiley, New York.
DeVor, R. E., Chang, T., and Sutherland, J. W., 1992, Statistical Quality Design and Control, Macmillan, New York.
Dornfield W.H. 1995. ``Direct Dynamic Testing of Scaled Stereolithographic Models," *Sound and Vibration*, August, pp. 12-17.
Fisher, T.S. et al. 1997. ``Analysis and Optimization of a Natural Draft Heat Sink System," IEEE Trans. On Components, Packaging, and Manufacturing Technology. Part A, Vol. 20, Number 2, pp.111-119
Holmes, M.F. 1984. ``Machine Dynamics, The Need for Greater Productivity", in K.N. Reid, ed., Research Needs in Mechanical Systems, ASME, NY, pp. 140-159.
Incropera, F.P. 1981, *Fundamentals of Heat Transfer*, John Wiley & Sons, New York.
Intel. 1998. ``Thermal Management", http://support.intel.com/support/processors/pentiumii/1793.htm/Thermal Management.
Jacobs, P. F. 1992. *Rapid Prototyping and Manufacturing: Fundamentals of StereoLithography*, Society of Manufacturing Engineers, McGraw-Hill Inc.
Kline, S.J. 1965. *Similitude and Approximate Theory*, McGraw-Hill, Inc.
Langhaar, H.L. 1951. *Dimensional Analysis and Theory of Models*, John Wiley and Sons, Inc., New York.
Linton, R.L. and Agonafer, D. 1995. ``Coarse and Detailed CFD Modeling of a Finned Heat Sink," In *Proceedings, 4th Intersociety Conf. on Thermal and Thermo Mechanical Phenomena in Electronic Systems*, Washington, DC
Nadworny, E.B. 1995. ``High Power CPU Cooling Experiment," In *Proceedings of the Computers in Engineering Conference and the Engineering Database Symposium*, ASME, Boston, MA, pp.1057-1066
O'Reilly, S.B. 1993. ``FFF at Ford Motor Company," In *Proceedings of the 1993 SFF Symposium*, Austin, TX, pp. 168-177.
Otto, K. and Wood, K. 2000. *Product Design*, Prentice-Hall, New York.
Pahl, G. and Beitz, W. 1984. *Engineering Design : A Systematic Approach*, The Design Council, Spring-Verlag, London.
Sedov, L.I. 1959. Similarity and Dimensional Methods in Mechanics, Academic Press, New York.
Strang, G. 1988. Linear Algebra and its Applications, Harcourt Brace Jovanovich, San Diego.
Szucs, E. 1980. *Similitude and Modeling*, Elsevier Scientific Publishing Company.
Ullman, D. 1992. *The Mechanical Design Process*, McGraw-Hill, New York.
Ulrich, K.T. and Eppinger, S.D. 1995. *Product Design and Development*, McGraw-Hill, Inc.
Wall, M.B. et al. 1991. ``Making Sense of Prototyping Technologies for Product Design," In Proceeding of ASME 3rd International Conference on Design Theory and Methodology, Vol.31, pp.157-164.
Wood, J. J., 2002, Design Methodology Using Empirical and Virtual Analysis with Application to Compliant Systems, Doctoral dissertation, Colorado State University.